surfaces

MDPI

Article

Using Highly Flexible SbSn@NC Nanofibers as Binderless Anodes for Sodium-Ion Batteries

Jiaojiao Liang [1,2], Gengkun Fang [1], Xinmiao Niu [1], Zhihao Zhang [1], Yufei Wang [1], Lingyuan Liao [1], Xiaoming Zheng [3], Di Huang [1,*] and Yuehua Wei [4,*]

[1] College of Railway Transportation, Hunan University of Technology, Zhuzhou 412008, China
[2] Qinghai Provincial Key Laboratory of Nanomaterials and Nanotechnology, Qinghai Minzu University, Qinghai 810007, China
[3] Hunan Provincial Key Laboratory of Intelligent Sensors and Advanced Sensor Materials, School of Physics and Electronics, Hunan University of Science and Technology, Xiangtan 411201, China
[4] School of Physics and Optoelectronics, Xiangtan University, Xiangtan 411105, China
* Correspondence: dihuang@hut.edu.cn (D.H.); weiyuehua18@nudt.com (Y.W.)

Abstract: Flexible and binderless electrodes have become a promising candidate for the next generation of flexible power storage devices. However, developing high-performance electrode materials with high energy density and a long cycle life remains a serious challenge for sodium-ion batteries (SIBs). The main issue is the large volume change in electrode materials during the cycling processes, leading to rapid capacity decay for SIBs. In this study, flexible electrodes for a SnSb alloy–carbon nanofiber (SnSb@NC) membrane were successfully synthesized with the aid of hydrothermal, electrospinning and annealing processes. The as-prepared binderless SnSb@NC flexible anodes were investigated for the storage properties of SIBs at 500 °C, 600 °C and 700 °C (SnSb@NC-500, SnSb@NC-600 and SnSb@NC-700), respectively. And the flexible SnSb@NC-700 electrode displayed the preferable SIB performances, achieving 240 mAh/g after 100 cycles at 0.1 A g^{-1}. In degree-dependent I-V curve measurements, the SnSb@NC-700 membrane exhibited almost the same current at different bending degrees of 0°, 45°, 90°, 120° and 175°, indicating the outstanding mechanical properties of the flexible binderless electrodes.

Keywords: SnSb alloy; sodium-ion batteries; anode; binderless; flexible

Citation: Liang, J.; Fang, G.; Niu, X.; Zhang, Z.; Wang, Y.; Liao, L.; Zheng, X.; Huang, D.; Wei, Y. Using Highly Flexible SbSn@NC Nanofibers as Binderless Anodes for Sodium-Ion Batteries. *Surfaces* **2023**, *6*, 239–248. https://doi.org/10.3390/surfaces6030016

Academic Editor: Gaetano Granozzi

Received: 29 May 2023
Revised: 25 June 2023
Accepted: 10 July 2023
Published: 16 July 2023

1. Introduction

Sodium-ion batteries (SIBs), as promising substitution candidates, have drawn much attention due to the account of the abundant sodium resources available, low cost and the outstanding safety performance [1–3]. However, the radius of Na ions is larger than that of Li ions, giving rise to serious volume expansion and slower sodiation/desodiation for the anode electrode [4–6]. This is the reason for the poor cycling capability and rate performance in SIBs. To improve the capacity of sodium storage, various anode materials have been studied, such as metals, transition-metal compounds, carbon materials and their composite materials [7–11]. Metal materials, especially Sn and Sb, exhibit an excellent performance because of the high theoretical capacity and low electrochemical potential window in SIBs [12–15]. Additionally, the theoretical capacity of metallic Sn can reach up to 847 mAh g^{-1} during its transformation into $Na_{15}Sn_4$ in the charge and discharge processes of SIBs, and the specific capacity of metallic Sb is approximately 660 mAh g^{-1}. Nevertheless, the large volume change in metallic Sn and Sb leads to the pulverization of electrodes for active materials, resulting in the attenuation of cycle stability and rate performance. Much effort has been made to reduce the shortcomings of metallic Sn and Sb and eventually enhance the performance of SIBs, including using nano-alloying metal to form SnSb alloys or composites with carbon materials [16–18]. SnSb alloy exhibits the

greater theoretical sodium storage capacity than Sn and Sb metals and can overcome the very active chemical properties of metallic sodium as anode materials [19].

With the rapid development of various flexible electronic products, such as wearable health-monitoring devices and foldable smartphones, it is urgent to develop flexible electrodes with excellent mechanical properties and high energy storage performance for SIBs [19–21]. Electrospinning, as one of the most simple and effective methods for preparing flexible and binderless electrodes, can be combined with high-temperature annealing under a reduction atmosphere to prepare one-dimensional metal–carbon composite nanofibers [22–26]. Zhang et al. used electrospinning to prepare flexible Sb/Sb_2O_3 films, delivering a high capacity and long, reversible cycle life (385.6 mAh g^{-1}/500 cycles) for SIBs [25]. Sadan et al. used a simple electrospinning and annealing method to prepare Sn embedded in carbon nanofibers as anode materials, and they found that the Sn CNF half-cell showed a stable long-term cycling performance of up to 30,000 cycles in SIBs [26]. Furthermore, one-dimensional carbon nanofibers can be used as a excellent flexible substrates on account of their special structure, outstanding electrical conductivity and stable electrochemical performance [27–30]. Nevertheless, the synthesis of flexible and binderless electrodes is adversely affected by the variation of conductivity and the flow regime of the precursor solvent during the direct one-step electrospinning method using raw metal salt [31]. Therefore, the smaller nanoalloys can be firstly acquired via the hydrothermal reaction and then added to the precursor solvent in the electrospinning process to form a suspension. Based on the process mentioned above, it can effectively prevent the direct use of metal salts to prepare flexible and binderless electrodes of carbon composites.

In this work, the flexible and binderless SnSb alloy–carbon nanofibers were successfully prepared through a hydrothermal reaction, electrospinning and annealing. To determine the effects of flexibility in SIBs, the sodium storage properties of the flexible SnSb alloy–carbon nanofiber electrodes were investigated systematically. And the influence of annealing temperatures on flexibility in SnSb alloy–carbon nanofibers was also optimized. Interestingly, flexible and binderless SnSb alloy–carbon nanofibers displayed a better sodium storage performance at 700 °C. Furthermore, the flexibility of SnSb@NC-700 electrodes was verified via bending-degree-related electric measurement. The changeless conductance of SnSb@NC-700 electrodes showed excellent flexibility.

2. Experimental Section

2.1. Material Preparation

2.1.1. Preparation of SnO_2 and Sb_2O_3 Nanomaterials

The SnO_2 and Sb_2O_3 nanomaterials were synthesized via the hydrothermal synthesis method, as follows: 2 mmol Tin(II) chloride ($SnCl_2$), 2 mmol antimony trichloride ($SbCl_3$) and 1 mmol cetyltrimethyl ammonium bromide (CTAB) were dissolved in mixed solvents composed of 20 mL of ethylene glycol and 20 mL of anhydrous ethanol. 3 mL of $NH_3 \cdot H_2O$ was slowly added into the above solution and stirred for 1 h. Then, the solution was transferred in a 50 mL Teflon-lined autoclave for a hydrothermal reaction with the temperature of 180 °C for 8 h. The precipitated products were collected and centrifugally cleaned with a mixture of deionized water and alcohol, and then dried at 60 °C overnight to obtain the mixed sample of SnO_2 and Sb_2O_3 nanomaterials.

2.1.2. Preparation of SnSb Alloy–Carbon Nanofibers

The synthesis of SnSb alloy–carbon nanofibers was carried out according to the following process: 0.7 g of polyacrylonitrile (PAN) was firstly added to 6 g of N, N-dimethylformamide (DMF) to form a faint yellow solution, and 0.4 g of mixed SnO_2 and Sb_2O_3 nanomaterials was dispersed in the above solution to create a suspension after continuous stirring and ultrasound. Then, the suspended solution was placed into a 10 mL injection pump, followed by electrospinning at a voltage of 12 kV to obtain a high voltage power and a distance of 15 cm between the collecting plate and the injection needle. The precursor flexible electrode of SnO_2, Sb_2O_3 and PAN was collected and vacuum-dried. Fur-

thermore, the preoxidized product was obtained after annealing at 150 °C for 8 h followed by 250 °C for 2 h under the air. Finally, the SnSb alloy–carbon nanofiber samples were obtained upon different annealing temperatures, namely 500 °C, 600 °C, 700 °C and 800 °C, for 2 h under an Ar/H_2 gas atmosphere, corresponding to SnSb@NC-500, SnSb@NC-600, SnSb@NC-700 and SnSb@NC-800, respectively.

2.2. Material Characterization

The crystal characteristics of all samples were analyzed with X-ray diffraction (XRD, D/Max 2500 Diffractometer, Rigaku, Japan.) after the hydrothermal, electrospinning and annealing processes, and the surface morphology and lattice constant of the samples were determined with scanning electron microscopy (SEM, S4800, Hitachi, Tokyo, Japan.) and a transmission electron microscope (TEM, FEI Tecnai F20 with an accelerating voltage of 200 kV, FEI, America.). The SnSb content in SnSb@NC-700 was determined via thermal gravimetric analysis (TGA, TGA 550, TA INSTRUMENTS, America.) under an air atmosphere from 20 °C to 800 °C. And the surface element composition of SnSb@NC-700 was analyzed with X-ray photoelectron spectroscopy (XPS, K-Alpha, Thermo Fisher Scientific, UK). Moreover, the current-voltage (I-V) curves of SnSb@NC-700 were measured with a high-precision digital source meter (IV2400) at different bending degrees.

2.3. Electrochemical Measurements

In order to investigate the sodium storage performance of flexible electrodes with SnSb alloy–carbon nanofibers, the SIBs anode was directly prepared with the film of SnSb alloy–carbon nanofibers after the experiment. The square-shaped electrode was approximately 1.0 cm × 1.0 cm, and the average weight of the flexible electrode was about 1.5 mg cm^{-2}. The electrochemical properties of the flexible electrodes for SnSb alloy–carbon nanofibers were tested using CR-2025-type coin cells, and metallic Na served as the counter electrode. An amount of 1.0 M $NaClO_4$ was mixed into an ethylene carbonate (EC) and diethyl carbonate (DEC) solution (with a weight ratio of 1:1) with 5% fluoroethylene carbonate (FEC) acting as an additive, which was used as the electrolyte of SIBs. A glass microfiber membrane (Whatman, grade GF/A, China.) was applied as the separator of SIBs. All of the button batteries were assembled in a glove box, where the water and oxygen contents were less than 0.01 ppm, respectively. The electrochemical performances were tested by means of a Neware battery test system (0.001–3 V) at different current densities, and the test voltage was between 0.001 and 3.0 V for Na^+/Na. Cyclic voltammetry (CV) was carried out in the same voltage window at the electrochemical work station.

3. Results and Discussions

The synthesis process diagram for flexible electrodes of SnSb alloy–carbon nanofibers is shown in Figure S1. Firstly, the mixed sample of SnO_2 and Sb_2O_3 was synthesized via a hydrothermal reaction, and the nanoparticles were observed in the morphology of the sample for SEM and are displayed in Figure S2. Via electrospinning, the precursor nanofibers of SnO_2 and Sb_2O_3 were obtained. In addition, the synthesis of flexible and binderless SnSb alloy–carbon nanofiber electrodes also required preoxidation and carbonization via annealing upon the air and reduction atmosphere. Under a high temperature and a reduction atmosphere (Ar/H_2), the SnSb alloy was created by SnO_2 and Sb_2O_3 in the flexible electrode. The 3D network of 1D carbon nanofibers containing nitrogen sources from the annealed PAN can further improve the conductivity of electrode materials [32–34]. Through hydrothermal, electrospinning and annealing processes, the flexible and binderless SnSb alloy–carbon nanofiber electrodes were prepared. After annealing at 800 °C, the material became brittle, exhibiting the poor flexibility. Therefore, SnSb@NC-500, SnSb@NC-600 and SnSb@NC-700 were studied via the characterization of these materials and their sodium storage properties.

In order to study the formation process and crystal structure of SnSb alloy–carbon nanofibers, XRD measurements were conducted, as displayed in Figure 1. SnO_2 and

Sb_2O_3 were verified via XRD after the hydrothermal reaction, as shown in Figure 1a. The patterns of the SnO_2 and Sb_2O_3 samples show diffraction peaks at 26.6°, 33.9°, 25.5° and 28.4° corresponding to the lattice planes (110), (101) of SnO_2 (powder diffraction file (PDF) No. 5-467) and (111), (121) of Sb_2O_3 (PDF No. 11-689), respectively. Electrospinning and annealing the SnSb@NC-500, SnSb@NC-600 and SnSb@NC-700 samples at 500 °C, 600 °C and 700 °C confirmed the existence of SnSb alloy in the SnSb alloy–carbon nanofibers, and the diffraction peaks of XRD at 29.1°, 41.5° and 41.7° correspond to lattice planes (101), (012) and (110) of SnSb (PDF No. 33-118), respectively. As the annealing temperature increased, the diffraction peaks became more evident, which may be ascribed to the higher crystallization and lattice defect degree of the SnSb alloy.

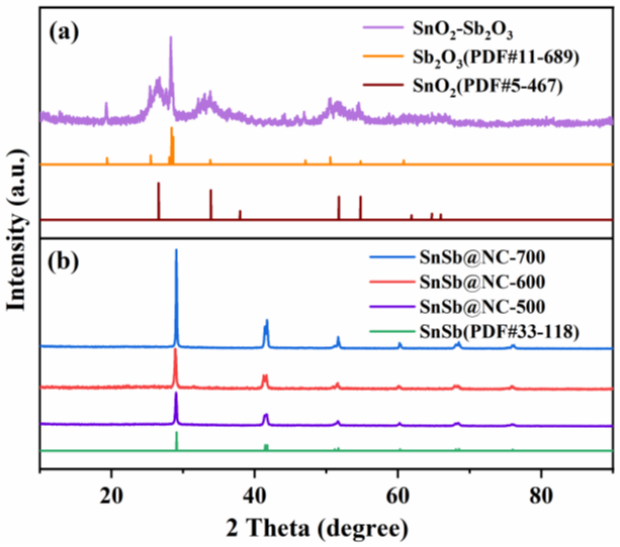

Figure 1. The XRD patterns of (**a**) SnO_2 and Sb_2O_3 samples and (**b**) SnSb alloy–carbon nanofibers.

The morphological characteristics of SnSb@NC-500, SnSb@NC-600 and SnSb@NC-700 were analyzed via SEM, the corresponding results are shown in Figure 2a–f. The 3D network structure composed of 1D homogeneous SnSb alloy–carbon nanofibers can be observed in the low-resolution SEM images of SnSb@NC-500, SnSb@NC-600 and SnSb@NC-700 (Figure 2a–c). From the high-resolution SEM images in Figure 2d–e, we can see that the diameter was approximately 450 nm. Additionally, there were no particles on the surface of SnSb alloy–carbon nanofibers, indicating that SnSb was probably encased in the carbon nanofibers. This result was also confirmed with TEM measurements, as shown in the low-resolution TEM image in Figure 2g. The wrinkling of the nanofibers became more obvious with the increase of the annealing temperature, due to the excellent degree of carbonization in PAN at higher temperatures. The 0.308 nm lattices corresponded to the interplanar spacing of the (101) plane and were encased in amorphous carbon material, observed in the high-resolution TEM image in Figure 2h. In order to analyze the SnSb content in SnSb@NC-700, a TGA test was executed under an air atmosphere from 20 °C to 800 °C, as displayed in Figure 2i. A slight weight loss around 20 °C to about 400 °C corresponded to the evaporation of crystal water in SnSb@NC-700. The subsequent weight variation from 200 °C to 580 °C may be due to the conversion of SnSb@NC-700 into CO_2, SnO_2 and Sb_2O_3. Then, the weight showed a slighter variation from 580 °C to 700 °C, which can be attributed to the transformation of Sb_2O_3 to Sb_2O_4 with oxygen gas [35]. Thus, the chemical equation for the whole process can be written as $2SnSb + C + nO_2 \rightarrow 2SnO_2 + Sb_2O_4 + CO_2\uparrow$. It can be observed that the final remaining mass was 45.5% of the total weight (m_{total}) in the SnSb@NC-700 composites, and the SnSb content was calculated to be 35.9%, according to the equation $m_{SnSb} = 2M_{SnSb} \times 45.5\%m_{total} \times (M_{Sb2O4} + 2M_{SnO2})^{-1}$.

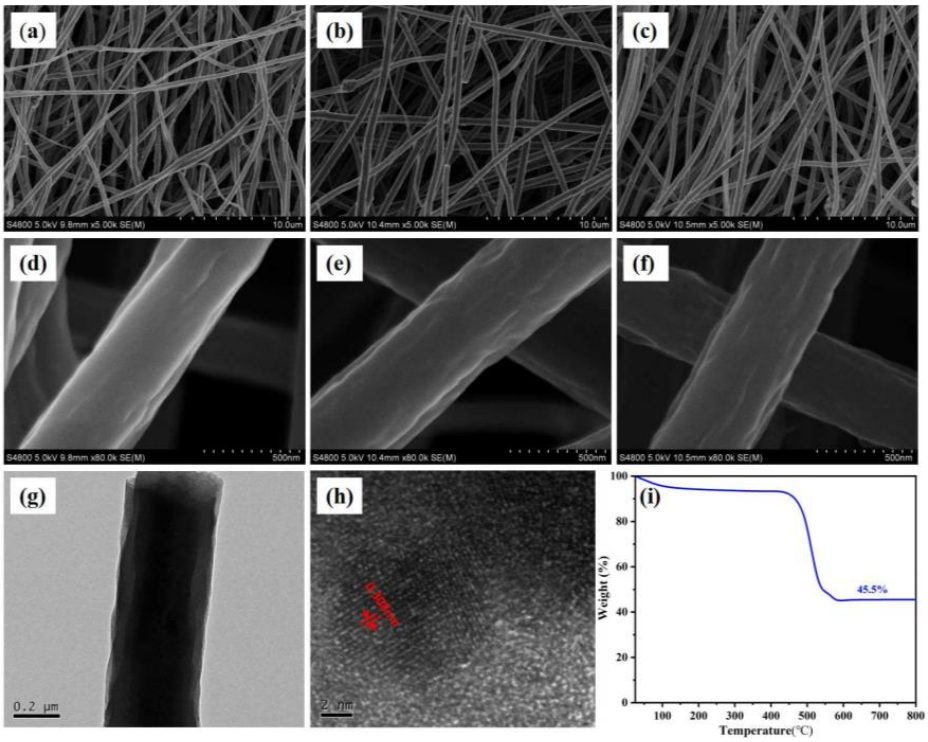

Figure 2. The SEM images of (**a**,**d**) SnSb@NC-500, (**b**,**e**) SnSb@NC-600 and (**c**,**f**) SnSb@NC-700; (**g**,**h**) the TEM images of SnSb@NC-700; (**i**) the TGA curve of SnSb@NC-700.

In order to further verify the specific electronic states of the components of SnSb@NC-700, X-ray photoelectron spectroscopy (XPS) was performed. The primary elements of Sb, Sn, N and C were observed in the low-resolution images (Figure S3). The XPS spectra of Sn 3d5/2 and 3d3/2 exhibited two main peaks at 487.0 and 495.4 eV and weak peaks at 485.1 and 497.3 eV in Figure 3a, which may correspond to Sn-C and tetravalent Sn [36]. The two peaks at 531.3 and 540.1 eV in Figure 3b can be assigned to Sb 3d5/2 and 3d3/2, and the other two peaks at 532.6 and 527.9 eV can be attributed to metallic Sb [37]. The C 1s spectrum in Figure 3c could be decomposed into four peaks, and the center energies of 284.6, 286.1, 288.5 and 290.5 eV corresponded to C=C, C-C, C-O and O=C-O, respectively [38]. The XPS spectrum of N1s in Figure 3d showed three peaks of pyrrolic N, pyridinic N and oxidized N at 398.2, 400.1 and 404.7 eV [39], correspondingly.

In addition, considering that the conductive property of SnSb@NC can be improved at higher temperatures, the conductivity of SnSb@NC-700 was investigated using a high-precision digital source meter at different bending degrees. And Photographs of the current–voltage (I-V) test for the SnSb@NC-700 membrane when bent at 0°, 45°, 90°, 120° and 175° are presented in Figure 4a–e. The corresponding I-V curves in Figure 4f almost coincide at different bending angles, indicating the unchangeable electrical conductivity of SnSb@NC-700 at various bending degrees. The good flexibility of SnSb@NC-700 was further demonstrated without any reduced conductivity.

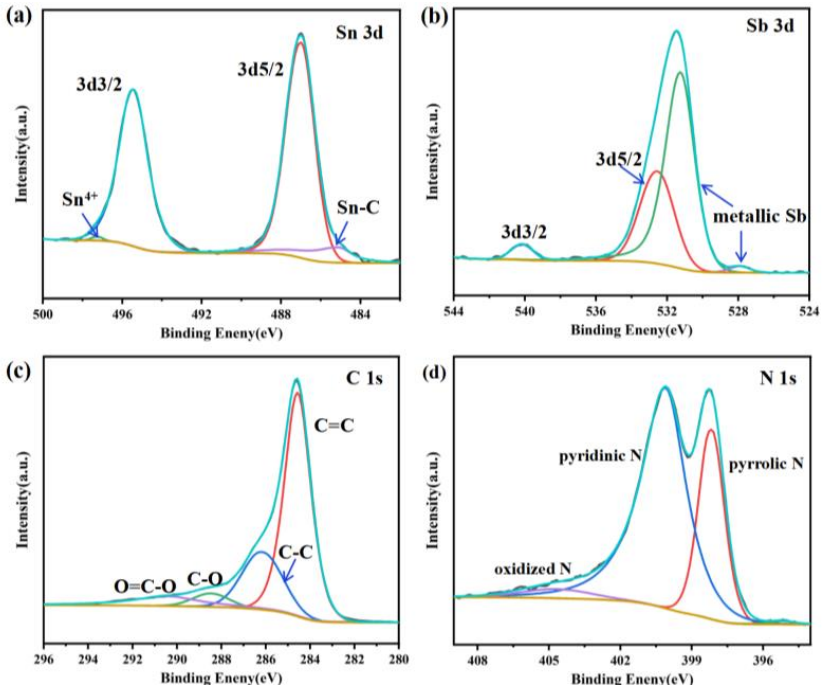

Figure 3. (**a**) The high-resolution XPS spectra of (**a**) Sn 3d, (**b**) Sb 3d, (**c**) C 1s and (**d**) N 1s.

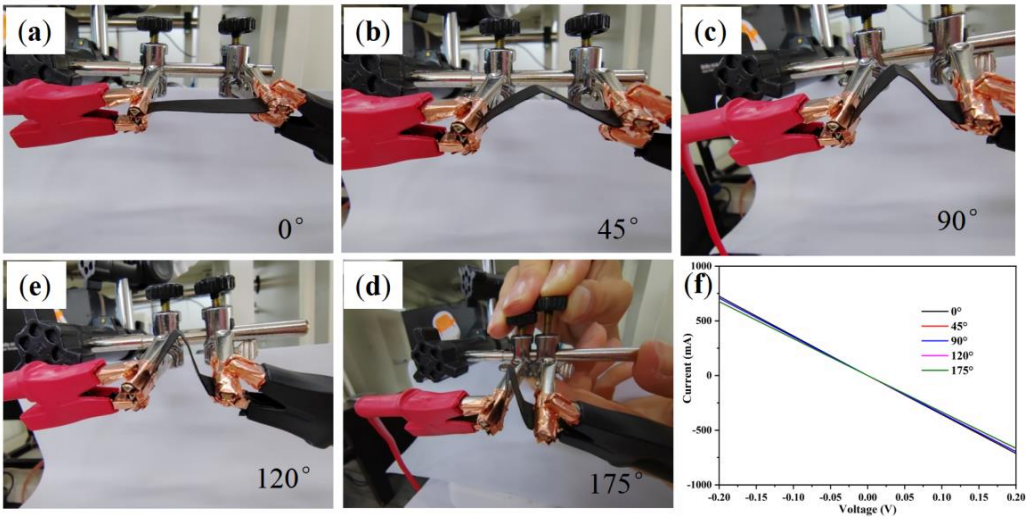

Figure 4. Photographs of SnSb@NC-700 during the current–voltage (I-V) test at different bending degrees: (**a**) 0°; (**b**) 45°; (**c**) 90°; (**d**) 120°; (**e**) 175°. (**f**) Corresponding curve diagrams of current–voltage (I-V).

The sodium storage properties of the flexible and binderless electrodes for SnSb@NC were assessed via cycling at a constant current and capacity at different current densities. The cycle performance of SIBs with SnSb@NC-700 electrodes displayed a higher reversible capacity than those of SIBs with SnSb@NC-600 electrodes and SnSb@NC-500 electrodes, as shown in Figure 5a. It is worth mentioning that SIBs with the flexible SnSb@NC-700 electrodes delivered a reversible capacity of 240 mAh g^{-1} at a constant current density of 0.1 A g^{-1} after 100 cycles, and the Coulomb efficiency was close to 100%. Additionally, it was easy to identify that our flexible storage device materials exhibited the comparable performance to the other SnSb-, Sb- and Sn-related flexible materials reported in the literature, as displayed in Table S1. And the charge–discharge curves of SnSb@NC-700 electrode are demonstrated in Figure S4 for 0.1 A g^{-1} at different cycles (1st, 2nd, 50th and

100th). Nevertheless, the reversible capacity of SnSb@NC-600 electrodes and SnSb@NC-500 electrodes was 180 mAh g^{-1} and almost 0 under the same conditions, respectively. Therefore, the SnSb@NC-700 electrodes display a better cycle performance. The rate capability of SnSb@NC-700 electrodes demonstrates they have a higher reversible capacity than SnSb@NC-600 electrodes and SnSb@NC-500 electrodes at various current densities, from 0.05 to 2 A g^{-1}, as shown in Figure 5b. In greater detail, average capacities of 320, 280, 240, 170, 80 and 10 mAh g^{-1} can be achieved at the current densities of 0.05, 0.1, 0.2, 0.5, 1 and 2 A g^{-1} for SIBs with SnSb@NC-700, respectively. Notably, when the current density returned to 0.1 A g^{-1}, the reversible capacity of SIBs was still 260 mAh g^{-1}, indicating the excellent performance of SnSb@NC-700 electrodes.

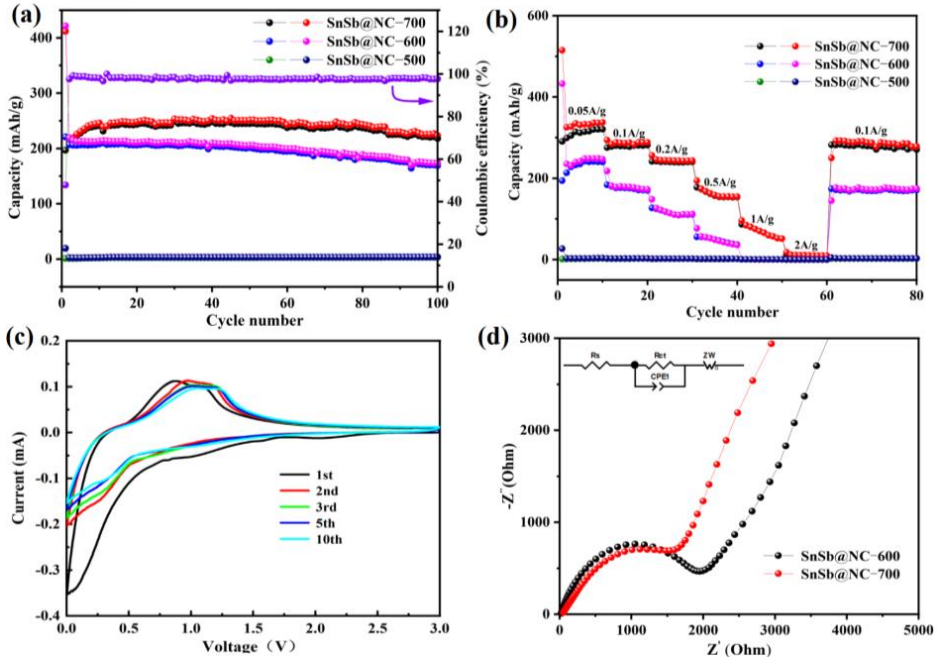

Figure 5. The sodium storage performance of flexible electrodes for SnSb alloy–carbon nanofibers at different annealing temperatures: (**a**) the cycle performance at 0.1 A/g; (**b**) the rate performance; (**c**) the cyclic voltammetry curves of SnSb@NC-700; and (**d**) the electrochemical impedance spectroscopy curve of SnSb@NC-600 and SnSb@NC-700.

The electrochemical properties of flexible SnSb@NC-700 electrodes used as the anodes for SIBs were analyzed using an electrochemical work station. Firstly, the cyclic voltammetry (CV) curves of flexible SnSb@NC-700 electrodes demonstrated their sodium-ion storage behavior by the 1st, 2nd, 3rd, 5th and 10th cycles at a voltage range of 0.001–3.0 V with a sweep rate of 0.1 mV s^{-1}, as displayed in Figure 5c. And a broad reduction peak was observed between 1.25 V and 0.8 V at the first cathodic scan curve, but it disappeared in subsequent scan curves. This may be due to the formation of a solid electrolyte interphase (SEI) film [36–38]. In the subsequent scan, reduction peaks at about 0.5 V and 0.2 V can be observed, which are associated with the alloying process allowing Sb to form Na_3Sb and Sn to form Na_xSn, respectively. And the two broad oxidation peaks at 0.25 V and 1.1 V corresponded to the formation process of Sb and Sn with the dealloying of Na_xSn and Na_3Sb [40–43]. Importantly, the peaks of the curves were very similar, exhibiting the unweakened sodium storage capacity and the similar alloying and dealloying processes for the SnSb@NC-700 electrodes after the subsequent scanning. To further confirm the reason for the better electrochemical performance, the electrochemical impedance spectroscopy (EIS) curves of SnSb@NC-700 and SnSb@NC-600 were investigated before the electrode cycle in Figure 5d. Obviously, the diameter of the semi-arc of SnSb@NC-700 electrodes was smaller than that of SnSb@NC-600 electrodes in the high-frequency area, indicating

the better electrical conductivity and diffusion kinetics of SnSb@NC-700 electrodes. Furthermore, the slope of the straight line of SnSb@NC-700 electrodes was a little steeper than that of SnSb@NC-600 electrodes in the low-frequency area, reflecting stronger Na^+ diffusion resistance. In addition, Zview software was used to simulate the equivalent circuit of EIS for SnSb@NC-700 and SnSb@NC-600, and the corresponding Rs of ohmic impedance and the Rct of interface impedance could be obtained, as shown in Table S2. The fitted impedance values of SnSb@NC-700 were smaller than those of SnSb@NC-600, which accorded with the EIS curve. Consequently, it can be concluded that SnSb@NC-700 electrodes are not only beneficial for the diffusion of sodium ions, but also contributed to the transfer of charge compared with SnSb@NC-600 electrodes [41].

4. Conclusions

In summary, the flexible electrodes of SnSb alloy–carbon nanofibers without a binder are formed via hydrothermal and electrospinning processes with excellent mechanical properties. And a 3D network structure composed of 1D homogeneous SnSb alloy–carbon nanofibers containing nitrogen can be used to improve the electrical conductivity and flexibly of the materials. The as-synthesized flexible, binderless anode SnSb@NC membrane displayed admirable storage properties for SIBs, and the reversible capacity of the flexible electrodes for SbSn@NC-700 was close to 240 mAh/g after 100 cycles. In addition, the flexible SbSn@NC-700 electrodes delivered average capacities of 320, 280, 240, 170, 80 and 10 mAh/g at the current densities of 0.05, 0.1, 0.2, 0.5, 1 and 2 A/g, respectively. Remarkably, they could still retain 260 mAh/g of reversible capacity when the current density returned to 0.1 A/g. Therefore, in this work, we have successfully developed a flexible electrode with an outstanding performance for SIBs.

Supplementary Materials: The following supporting information can be downloaded at: https://www.mdpi.com/article/10.3390/surfaces6030016/s1. Figure S1: The schematic diagram synthesis of flexible SnSb carbon composite; Figure S2: The SEM of the mix sample for SnO_2 and Sb_2O_3 nanomaterials; Figure S3: The low-resolution XPS spectra of SnSb@NC-700; Figure S4: The charge/discharge curve of SnSb@NC-700 electrode at different cycles (1st, 2nd, 50th, and 100th); Table S1: Compare with other SnSb, Sb, Sn related flexible materials reported in storage device; Table S2: The fitted impedance parameters of the material. References [25,26,41,42] are cited in the supplementary materials.

Author Contributions: Conceptualization, J.L.; Data curation, J.L., G.F. and X.N.; Funding acquisition, J.L. and D.H.; Investigation, J.L., G.F., X.N., Z.Z. and Y.W. (Yufei Wang); Project administration, J.L. and G.F.; Resources, L.L., X.Z., D.H. and Y.W. (Yuehua Wei); Supervision, D.H.; Validation, J.L., L.L., X.Z. and Y.W. (Yuehua Wei); Visualization, J.L., L.L., X.Z., D.H. and Y.W. (Yuehua Wei); Writing—original draft, J.L.; Writing—review and editing, D.H. and Y.W. (Yuehua Wei). All authors have read and agreed to the published version of the manuscript.

Funding: This research was funded by the Natural Science Foundation of Hunan Province, grant number 2021JJ40168 and 2020JJ5135, the Education Department of Hunan Province, grant number 21B0534 and 22B0580, the Qinghai Provincial Laboratory of Nanomaterials and Nanotechnology, grant number 2022-QHMD-PI-NM-03, and the National Innovation and Entrepreneurship Training Project for College Students, grant number 202211535013.

Institutional Review Board Statement: Not applicable.

Informed Consent Statement: Not applicable.

Data Availability Statement: The data are available in the Supporting Information.

Acknowledgments: This work was financially supported by the Natural Science Foundation of Hunan Province (grant no. 2021JJ40168 and 2020JJ5135), the Education Department of Hunan Province (grant no. 21B0534 and 22B0580), The Open Fund Project of Qinghai Provincial Laboratory of Nanomaterials and Nanotechnology, no. 2022-QHMD-PI-NM-03, and the National Innovation and Entrepreneurship Training Project for College Students (No. 202211535013).

Conflicts of Interest: There are no conflicts to declare.

References

1. Wu, D.; Zhu, C.; Wu, M.; Wang, H.; Huang, J.; Tang, D.; Ma, J. Highly Oxidation-Resistant Electrolyte for 4.7 V Sodium Metal Batteries Enabled by Anion/Cation Solvation Engineering. *Angew. Chem. Int. Ed.* **2022**, *61*, e202214198. [CrossRef] [PubMed]
2. Xia, Q.; Liu, H.; Zhao, X.S. Surface engineering of anode materials for improving sodium-ion storage performance. *J. Mater. Chem. A* **2022**, *10*, 3889–3904. [CrossRef]
3. Lei, D.; He, Y.-B.; Huang, H.; Yuan, Y.; Zhong, G.; Zhao, Q.; Hao, X.; Zhang, D.; Lai, C.; Zhang, S.; et al. Cross-linked beta alumina nanowires with compact gel polymer electrolyte coating for ultra-stable sodium metal battery. *Nat. Commun.* **2019**, *10*, 4244. [CrossRef]
4. Liang, J.; Wei, Z.; Wang, C.; Ma, J. Vacancy-induced sodium-ion storage in N-doped carbon Nanofiber@MoS2 nanosheet arrays. *Electrochim. Acta* **2018**, *285*, 301–308. [CrossRef]
5. Li, S.; He, W.; Liu, B.; Cui, J.; Wang, X.; Peng, D.-L.; Liu, B.; Qu, B. One-step construction of three-dimensional nickel sulfide-embedded carbon matrix for sodium-ion batteries and hybrid capacitors. *Energy Storage Mater.* **2019**, *25*, 636–643. [CrossRef]
6. Zhang, Y.; Tang, D.; Liu, Y.; Wang, J.; Li, Z.; Li, X.; Han, G.; Wei, Q.; Qu, B. Sodium Stoichiometry Tuning of the Biphasic-Na_xMnO_2 Cathode for High-Performance Sodium-Ion Batteries. *Small* **2023**, *61*, e2301141. [CrossRef]
7. Liang, J.; Fan, K.; Wei, Z.; Gao, X.; Song, W.; Ma, J. Porous NaTi2(PO4)3@C nanocubes as improved anode for sodium-ion batteries. *Mater. Res. Bull.* **2018**, *99*, 343–348. [CrossRef]
8. Qi, S.; Wu, D.; Dong, Y.; Liao, J.; Foster, C.W.; O'Dwyer, C.; Feng, Y.; Liu, C.; Ma, J. Cobalt-based electrode materials for sodium-ion batteries. *Chem. Eng. J.* **2019**, *370*, 185–207. [CrossRef]
9. Wang, L.; Yang, C.; Dou, S.; Wang, S.; Zhang, J.; Gao, X.; Ma, J.; Yu, Y. Nitrogen-doped hierarchically porous carbon networks: Synthesis and applications in lithium-ion battery, sodium-ion battery and zinc-air battery. *Electrochim. Acta* **2016**, *219*, 592–603. [CrossRef]
10. Wang, L.; Wei, Z.; Mao, M.; Wang, H.; Li, Y.; Ma, J. Metal oxide/graphene composite anode materials for sodium-ion batteries. *Energy Storage Mater.* **2019**, *16*, 434–454. [CrossRef]
11. Chen, C.; Yang, Y.; Tang, X.; Qiu, R.; Wang, S.; Cao, G.; Zhang, M. Graphene-Encapsulated FeS_2 in Carbon Fibers as High Reversible Anodes for Na^+/K^+ Batteries in a Wide Temperature Range. *Small* **2019**, *15*, e1804740. [CrossRef]
12. Liang, J.-M.; Zhang, L.-J.; Xili, D.-G.; Kang, J. Research progress on tin-based anode materials for sodium ion batteries. *Rare Met.* **2020**, *39*, 1005–1018. [CrossRef]
13. Luo, W.; Gaumet, J.-J.; Mai, L.-Q. Antimony-based intermetallic compounds for lithium-ion and sodium-ion batteries: Synthesis, construction and application. *Rare Met.* **2017**, *36*, 321–338. [CrossRef]
14. Jing, W.T.; Yang, C.C.; Jiang, Q. Recent progress on metallic Sn- and Sb-based anodes for sodium-ion batteries. *J. Mater. Chem. A* **2020**, *8*, 2913–2933. [CrossRef]
15. Sarkar, S.; Peter, S.C. An overview on Sb-based intermetallics and alloys for sodium-ion batteries: Trends, challenges and future prospects from material synthesis to battery performance. *J. Mater. Chem. A* **2021**, *9*, 5164–5196. [CrossRef]
16. Li, L.; Seng, K.H.; Li, D.; Xia, Y.; Liu, H.K.; Guo, Z. SnSb@carbon nanocable anchored on graphene sheets for sodium ion batteries. *Nano Res.* **2014**, *7*, 1466–1476. [CrossRef]
17. Walter, M.; Doswald, S.; Kovalenko, M.V. Inexpensive colloidal SnSb nanoalloys as efficient anode materials for lithium- and sodium-ion batteries. *J. Mater. Chem. A* **2016**, *4*, 7053–7059. [CrossRef]
18. Jia, H.; Dirican, M.; Chen, C.; Zhu, J.; Zhu, P.; Yan, C.; Li, Y.; Dong, X.; Guo, J.; Zhang, X. Reduced graphene oxide-incorporated SnSb@CNF composites as anodes for high-performance sodium-ion batteries. *ACS Appl. Mater. Interfaces* **2018**, *10*, 9696–9703. [CrossRef]
19. Li, H.; Zhang, X.; Zhao, Z.; Hu, Z.; Liu, X.; Yu, G. Flexible sodium-ion based energy storage devices: Recent progress and challenges. *Energy Storage Mater.* **2019**, *26*, 83–104. [CrossRef]
20. Mishra, K.; Yadav, N.; Hashmi, S.A. Recent progress in electrode and electrolyte materials for flexible sodium-ion batteries. *J. Mater. Chem. A* **2020**, *8*, 22507–22543. [CrossRef]
21. Tang, X.; Yan, F.; Wei, Y.; Zhang, M.; Wang, T.; Zhang, T. Encapsulating Sn_xSb Nanoparticles in Multichannel Graphene-Carbon Fibers As Flexible Anodes to Store Lithium Ions with High Capacities. *ACS Appl. Mater. Interfaces* **2015**, *7*, 21890–21897. [CrossRef] [PubMed]
22. Sun, B.; Long, Y.-Z.; Chen, Z.-J.; Liu, S.-L.; Zhang, H.-D.; Zhang, J.-C.; Han, W.-P. Recent advances in flexible and stretchable electronic devices via electrospinning. *J. Mater. Chem. C* **2013**, *2*, 1209–1219. [CrossRef]
23. Wang, J.; Wang, Z.; Ni, J.; Li, L. Electrospinning for flexible sodium-ion batteries. *Energy Storage Mater.* **2022**, *45*, 704–719. [CrossRef]
24. Xiong, Q.; He, H.; Zhang, M. Design of Flexible Films Based on Kinked Carbon Nanofibers for High Rate and Stable Potassium-Ion Storage. *Nano-Micro Lett.* **2022**, *14*, 47. [CrossRef] [PubMed]
25. Zhang, L.; Song, Y.; Hu, Y.; Ruan, H.; Bai, J.; Li, S.; Liu, Y.; Guo, S. Flexible Sb/Sb_2O_3-C nanofibers as binder-free anodes for high-performance and stable sodium-ion batteries. *J. Alloys Compd.* **2021**, *890*, 161913. [CrossRef]
26. Sadan, M.K.; Kim, H.; Kim, C.; Cho, G.-B.; Cho, K.-K.; Ahn, J.-H.; Ahn, H.-J. Ultra-long cycle life of flexible Sn anode using DME electrolyte. *J. Alloys Compd.* **2021**, *871*, 159549. [CrossRef]

27. Zhang, Q.; Zeng, Y.; Ling, C.; Wang, L.; Wang, Z.; Fan, T.; Wang, H.; Xiao, J.; Li, X.; Qu, B. Boosting Fast Sodium Ion Storage by Synergistic Effect of Heterointerface Engineering and Nitrogen Doping Porous Carbon Nanofibers. *Small* **2022**, *18*, 2107514. [CrossRef]
28. He, H.; Lian, J.; Chen, C.; Xiong, Q.; Li, C.C.; Zhang, M. Enabling Multi-Chemisorption Sites on Carbon Nanofibers Cathodes by an In-situ Exfoliation Strategy for High-Performance Zn–Ion Hybrid Capacitors. *Nano-Micro Lett.* **2022**, *14*, 106. [CrossRef] [PubMed]
29. Huang, D.; Wu, D.; Zhu, J.; Xie, J.; Wu, J.; Liang, J. One-dimensional ZnSe@N-doped carbon nanofibers with simple electrospinning route for superior Na/K-ion storage. *Chin. Chem. Lett.* **2023**, *34*, 107416. [CrossRef]
30. Wang, H.; Yang, X.; Wu, Q.; Zhang, Q.; Chen, H.; Jing, H.; Wang, J.; Mi, S.-B.; Rogach, A.L.; Niu, C. Encapsulating Silica/Antimony into Porous Electrospun Carbon Nanofibers with Robust Structure Stability for High-Efficiency Lithium Storage. *ACS Nano* **2018**, *12*, 3406–3416. [CrossRef]
31. Joshi, B.; Samuel, E.; Kim, Y.-I.; Yarin, A.L.; Swihart, M.T.; Yoon, S.S. Progress and potential of electrospinning-derived substrate-free and binder-free lithium-ion battery electrodes. *Chem. Eng. J.* **2021**, *430*, 132876. [CrossRef]
32. Liu, B.; Lei, D.; Wang, J.; Zhang, Q.; Zhang, Y.; He, W.; Zheng, H.; Sa, B.; Xie, Q.; Peng, D.-L.; et al. 3D uniform nitrogen-doped carbon skeleton for ultra-stable sodium metal anode. *Nano Res.* **2020**, *13*, 2136–2142. [CrossRef]
33. Zhao, Y.; Liang, J.; Wang, C.; Ma, J.; Wallace, G.G. Tunable and Efficient Tin Modified Nitrogen-Doped Carbon Nanofibers for Electrochemical Reduction of Aqueous Carbon Dioxide. *Adv. Energy Mater.* **2018**, *8*, 1702524. [CrossRef]
34. Liang, J.; Yuan, C.; Li, H.; Fan, K.; Wei, Z.; Sun, H.; Ma, J. Growth of SnO_2 Nanoflowers on N-doped Carbon Nanofibers as Anode for Li- and Na-ion Batteries. *Nano-Micro Lett.* **2017**, *10*, 21. [CrossRef] [PubMed]
35. Dang, J.; Zhu, R.; Zhang, S.; Yang, L.; Chen, X.; Wang, H.; Liu, X. Bean Pod-Like SbSn/N-Doped Carbon Fibers toward a Binder Free, Free-Standing, and High-Performance Anode for Sodium-Ion Batteries. *Small* **2022**, *18*, 2107869. [CrossRef]
36. Zhang, Y.; Sun, L.; Zhao, X.; Wu, L.; Wang, K.; Si, H.; Gu, J.; Sun, C.; Shi, Y.; Zhang, Y. Construction of Sn–P–graphene microstructure with Sn–C and P–C co-bonding as anodes for lithium-ion batteries. *Chem. Commun.* **2020**, *56*, 10572–10575. [CrossRef]
37. Dai, C.; Zhou, Z.; Zhou, X.; Zhang, Y. Removal of Sb(III) and Sb(V) from Aqueous Solutions Using nZVI. *Water Air Soil Pollut.* **2013**, *225*, 1799. [CrossRef]
38. Zhou, X.; Zhang, Z.; Xu, X.; Yan, J.; Ma, G.; Lei, Z. Anchoring Sb_6O_{13} nanocrystals on graphene sheets for enhanced lithium storage. *ACS Appl. Mater. Interface* **2016**, *8*, 35398–35406. [CrossRef]
39. Javed, R.; Khan, M.A.; Ye, D.; Zhao, Y.; Shah, L.A.; Zhang, J.; Zhao, H. Boosting Oxygen Reduction Catalysis Through Electronic Reconfiguration of Fe–N–C Induced by P Doping. *Electrocatalysis* **2021**, *12*, 747–758. [CrossRef]
40. Cheng, D.; Wei, A.; Ye, L.; Xu, G.; Tan, L.; Lu, B.; Chen, Y. Interfacial Bonding of SnSb Alloys with Graphene toward Ultrafast and Cycle-Stable Na-Ion Battery Anodes. *ACS Sustain. Chem. Eng.* **2022**, *10*, 12177–12187. [CrossRef]
41. Yang, L.; Yang, B.; Chen, X.; Wang, H.; Dang, J.; Liu, X. Bimetallic alloy SbSn nanodots filled in electrospun N-doped carbon fibers for high performance Na-ion battery anode. *Electrochim. Acta* **2021**, *389*, 138246. [CrossRef]
42. Song, Z.; Wang, G.; Chen, Y.; Lu, Y.; Wen, Z. In situ three-dimensional cross-linked carbon nanotube-interspersed SnSb@CNF as freestanding anode for long-term cycling sodium-ion batteries. *Chem. Eng. J.* **2023**, *463*, 142289. [CrossRef]
43. Jia, H.; Dirican, M.; Zhu, J.; Chen, C.; Yan, C.; Zhu, P.; Li, Y.; Guo, J.; Caydamli, Y.; Zhang, X. High-performance SnSb@rGO@CMF composites as anode material for sodium-ion batteries through high-speed centrifugal spinning. *J. Alloys Compd.* **2018**, *752*, 296–302. [CrossRef]